To appear in *Molecular Physics*
Vol. 00, No. 00, Month 200x, 1–24

RESEARCH ARTICLE

Applications to metal K pre-edges of transition metal dimers illustrate the approximate origin independence for the intensities in the length representation

Lasse Kragh Sørensen[a*], Meiyuan Guo[a], Roland Lindh[a,b] and Marcus Lundberg[a**]

[a] *Department of Chemistry - Ångström Laboratory, Uppsala University, S-75105 Uppsala, Sweden*; [b] *Uppsala Center of Computational Chemistry - UC$_3$, Uppsala University, S-75105 Uppsala, Sweden*

(*v1.0 submitted january 2016*)

Keywords: Multiconfigurational wavefunction, Oscillator Strengths, Quadrupole intensities, Properties, X-ray Spectroscopy

X-ray absorption spectroscopy (XAS) in the metal K pre-edge is a standard probe of electronic and geometric structure of transition metal complexes. Simulating the K pre-edge spectra require contributions beyond the electric dipole, but if that term is non-zero, the second-order terms, e.g., electric quadrupoles, are no longer origin independent. In the velocity representation, complete origin independence can be achieved by including all terms to the same order in the oscillator strength. Here we implement that approach in the length representation and use it for restricted active space (RAS) simulations of metal K pre-edges of iron monomers and dimers. Complete origin independence is not achieved and the size of the remaining errors depend on the electric dipole oscillator strength and its ratio in length and velocity representations. The error in the origin independence is in the ANO basis sets two orders of magnitude smaller than the value of the individual contributions. For systems with strong electric dipole contributions the errors are not significant within 3$\mathring{A}$ from a metal center, far enough to handle many multi-metal systems. Furthermore, we discuss the convergence of the multipole expansion, the possibility to assign spectral contributions, and the origin of negative absorption intensities.

*Corresponding author. Email: lasse.kraghsorensen@kemi.uu.se

**Corresponding author. Email: marcus.lundberg@kemi.uu.se

ISSN: 0040-5167 print/ISSN 1754-2278 online

DOI: 10.1080/0040516YYxxxxxxxx
http://www.informaworld.com

1. Introduction

The electronic and geometric structure of transition metal enzymes and solution catalysts can be probed *in situ* using hard X-rays. The metal K-edge is dominated by electric-dipole allowed $1s$ to $4p$ transitions, while the electric-quadrupole allowed $1s$ to $3d$ transitions make up the metal K pre-edge. The latter transitions give information about electronic structure. e.g., oxidation state, spin multiplicity and ligand-field strength.[1] The pre-edge is sensitive to geometric structure as distortions from centrosymmetry allow for $4p$ orbital character to mix into the valence orbitals, thus adding contributions from dipole-allowed transitions into the pre-edge.[2]

Distortions that change the pre-edge intensity are changes from six- to five- or four-coordinate tetrahedral sites. [1, 3] Another alternative is the presence of a strongly binding ligand, e.g., the metal-oxo groups proposed to be the reactive species in many enzymatic and synthetic systems.[4–7] Oxo groups also appear as bridging ligands in many bi- and multinuclear transition metal complexes.

An electronic structure approach that is well suited for transition metal systems is the multi-configurational self-consistent field (MCSCF) method, among which the complete active space (CAS) SCF version is the most widely used.[8] The MCSCF method has also been frequently used to calculate X-ray spectra as pioneered by Jensen and Ågren. [9–11] They showed how a fully optimized core hole can be obtained for an MCSCF wavefunction without variational collapse by first optimizing the wavefunction with the core orbital frozen and then using a second-order optimization algorithm to ensure convergence to a local minimum.[9, 12] Further, they showed how to efficiently calculate transition intensities for both photoelectron and radiative transitions with orbitals that are optimized separately for ground and core-excited states by taking advantage of the biorthogonalization scheme of Malmqvist.[10, 11, 13]

Recently, the restricted active space (RAS) SCF and PT2 methods have been used to model metal L-edge XAS spectra of a variety of transition metal complexes using the electric dipole approximation.[14–20]. For metal K-edge XAS, in particular the pre edge, the dipole approximation no longer suffices and electric quadrupole and magnetic dipole contributions are therefore also considered. We showed that the RAS method can also be used to accurately model iron K pre-edge spectra, including the effects of $3d$-$4p$ orbital hybridization that leads to a mix of electric dipole and quadrupole transitions, as well as those from multiplet interactions and spin-orbit coupling.[21] These calculations were made on mononuclear systems with the metal in the centre of symmetry.

However,for transitions with non-zero dipole contributions the electric quadrupole and magnetic dipole transitions are, however, origin-dependent. This becomes important for multi-metal systems since these systems lack a natural expansion point. Extending the RAS method to a wider set of molecular systems, including those with multiple metal centers, requires a better understanding of the origin dependence of the second-order transitions.

In the calculation of transition probabilities a Taylor expansion of the exponential form of the wave vector into electric dipole and higher order terms is usually performed. Bernadotte et al.[22] showed that full origin independence of the oscillator strengths can be achieved by including all terms of a given order in the expansion of the observable oscillator strength and not in the transition moments, and implemented this approach for time-dependent density-functional theory (TD-DFT) calculations of K edges. The electric dipole is the only contribution to the zeroth-order expansion. The second order, typically associated with electric quadrupole

and magnetic dipole interactions, also requires the calculation of electric octopoles and magnetic quadrupoles because they couple with the low-order electric dipole transitions. We have implemented this scheme in the restricted active space state interaction (RASSI) method to calculate oscillator strengths between non-orthogonal RASSCF and RASPT2 states.

Another possibility is to avoid the multipole expansion and use the exponential form of the wave vector as a perturbation where the integral of the exact expression is evaluated using the Euler formulas.[23] However, this requires the calculation of new types of integrals that are not readily available in most codes. An isotropic tensor averaging, known from the terms in the multipole expansion, is not known for the exponential form of the wave vector. Obtaining expressions for the isotropically averaged oscillator strengths for the exponential form of the wave vector instead needs to be performed by introducing a Lebedev grid [24].

When calculating transition probabilities, it is usually assumed that the electromagnetic field is weak and therefore can be treated as a perturbation to the stationary Hamiltonian $\hat{H}_0$. Wavefunction metods, with exception of full configuration interaction (FCI) in the complete basis set limit, only provide approximate solutions to the electronic structure problem. It has been argued that the use of non-exact eigenfunctions of $\hat{H}_0$ gives transition moments that are not exact and hence origin independence cannot be guaranteed, independent of the form of the perturbation. It can, however be shown that the origin independence is always guaranteed in the velocity representation irrespectively of the choice of $\hat{H}_0$, basis set and level of correlation treatment even when using the multipole expansion [25]. In the theory section we will here clarify the arguments for why the convergence of the multipole expansion does not depend on the choice of origin as claimed [26] and comment on the interpretation of spectra since the latter is often performed in the origin dependent terms.

However, an important detail is that the expansion of the origin-independent formulation in reference [22] is only strictly valid in the velocity representation. Transformation to the length representation is typically done through commutator relations, which, however, requires that these hold exactly. Our implementation, as most other quantum chemistry codes, is in the length representation and origin-independence can thus not be guaranteed even when using the complete second-order expansion of the wave vector.

To analyze the stability of second-order oscillator strengths for approximate wavefunctions, these have been calculated for four different model systems. First, the basic principles are outlined with the use of the spherically symmetric Fe^{3+} atomic system where the pre-edge has no dipole contribution. This is followed by $[FeCl_4]^{1-}$ where the dipole contributions to the metal K pre-edge are strong, but where the metal is in the centre of symmetry. The remaining two models are both biferric systems with an oxo bridge, the three-atom $[Fe_2O]^{4+}$ core and the [(hedta)FeOFe(hedta)] iron dimer. They both have dipole contributions in the pre-edge and at least one metal center away from the origin. The negative oscillator strengths previously observed [27] are also here observed. Since the negative intensities are only observed in some basis sets for the same system we ascribe the negative oscillator strengths to basis set deficiency and not to the lack of higher order in the multipole expansion since the different terms in the multipole expansion have different basis set requirements and the different terms can therefore individually be over- or underestimated.

2. Theory

In this section we breifly recapitulate the findings by Bernadotte et al.[22] essential for our implementation and application. The notation will be kept the same and we will refer the reader to reference [22] for derivations. This implementation is for the isotropically averaged second order intensities $f_{0n}^{(2)}$ which are colloquially called quadrupole intensities and this term will also be used in the proceeding text.

2.1. *The electromagnetic field as a perturbation*

It is thoughout assumed that the electromagnetic fields are weak and can be treated as a perturbation of the molecular system

$$\hat{H} = \hat{H}_0 + \hat{U}(t) \tag{1}$$

where the zeroth order Hamiltonian $\hat{H}_0$, in this derivation, is a molecular system described by the Schrödinger equation within the Born-Oppenheimer approximation

$$\hat{H}_0 = \sum_{i=1}^{N} \frac{\hat{\boldsymbol{p}}_i^2}{2m_e} + V(\boldsymbol{r}_1, \ldots, \boldsymbol{r}_N) \tag{2}$$

and $\hat{U}(t)$ is the time-dependent perturbation

$$\hat{U}(t) = \hat{U} exp(-\imath\omega t) + \hat{U}^* exp(\imath\omega t) \tag{3}$$

where $\hat{U}$ is the time-independent part of the perturbation

$$\hat{U} = \frac{eA_0}{2m_e c} \sum_i \left[exp(\imath \boldsymbol{k} \cdot \boldsymbol{r}_i)(\boldsymbol{\mathcal{E}} \cdot \hat{\boldsymbol{p}}_i) + \imath \frac{g}{2} exp(\imath \boldsymbol{k} \cdot \boldsymbol{r}_i)(\boldsymbol{k} \times \boldsymbol{\mathcal{E}}) \cdot \hat{\boldsymbol{s}}_i \right]. \tag{4}$$

In Eq. 4 $\boldsymbol{k}$ is the wave vector pointing in the direction of propagation, $\boldsymbol{\mathcal{E}}$ the polarization vector perpendicular to $\boldsymbol{k}$ and ω, in Eq. 3, is the angular frequency which is related to the frequency ν as $\omega = 2\pi\nu$. The second term in Eq. 4 describing the interaction with the spin $\hat{\boldsymbol{s}}$ is in the following omitted.

By applying Fermi's golden rule and assuming that transitions only occur when the energy difference between the eigenstates of the unperturbed molecule matches the frequency of the perturbation

$$\omega = \omega_{0n} = \frac{E_n - E_0}{\hbar}, \tag{5}$$

where 0 and n is the starting and final state, respectively, the explicit time dependence can be eliminated from the transition rate

$$\Gamma_{0n}(\omega) = \frac{2\pi}{\hbar} |\langle 0|\hat{U}|n\rangle|^2 \delta(\omega - \omega_{0n}) = \frac{\pi A_0^2}{2\hbar c} |T_{0n}|^2 \delta(\omega - \omega_{0n}). \tag{6}$$

In Eq. 6 the transition moments T_{0n} have been introduced and the effect of the weak time-dependent electromagnetic field can now be expressed as a time-independent expectation value.

2.2. *Origin independence of the oscillator strengths*

Bernadotte et al.[22] showed that origin independence in the oscillator strengths f_{0n}

$$f_{0n} = \frac{2m_e}{e^2 E_{0n}} |T_{0n}|^2, \tag{7}$$

where $E_{0n} = E_n - E_0$ is the difference in the energy of the eigenstates of the unperturbed molecule, comes naturally provided that the collection of the terms in Taylor expansion of the exponential of the wave vector $\boldsymbol{k}$

$$exp(\imath \boldsymbol{k} \cdot \boldsymbol{r}_i) = 1 + \imath(\boldsymbol{k} \cdot \boldsymbol{r}_i) - \frac{1}{2}(\boldsymbol{k} \cdot \boldsymbol{r}_i)^2 + \ldots \tag{8}$$

is collected to the same order in the observable oscillator strengths f_{0n}

$$f_{0n} = f_{0n}^{(0)} + f_{0n}^{(1)} + f_{0n}^{(2)} + \ldots \tag{9}$$

in Eq. 7 and not in the transition moments T_{0n}

$$T_{0n} = T_{0n}^{(0)} + T_{0n}^{(1)} + T_{0n}^{(2)} + \ldots \tag{10}$$

traditionally done. Hence when the multipole expansion for the transition moments in Eq. 10 is inserted in the expression for the oscillator strength in Eq. 7

$$f_{0n} = \frac{2m_e}{e^2 E_{0n}} |T_{0n}^{(0)} + T_{0n}^{(1)} + T_{0n}^{(2)} + \ldots|^2 \tag{11}$$

the truncation should be to the same order in the observable oscillator strengths f_{0n}.

The choice of origin for the coordinate system in the velocity representation can be choosen completely freely and will give exactly the same result when all terms to a given order in the oscillator strengths are included due to exact cancellation. Hence there will never be a choice of origin where the Taylor expansion in Eq. 8 will converge faster than any other choice of origin as claimed in [26] and repeated in [27]. The only difference between the different choices of origin is the size of the terms in the exact cancellation.

The concern about the different interpretations and assignments of spectral features in terms of orders of electric and magnetic contributions as raised in [27] stems from trying to interpret transitions in terms of non-observable transitions with a given choice of origin. Only the total oscillator strengths are observable, the individual contributions are not. For the origin independent oscillator strengths the change of origin will leave every order in oscillator strength in Eq. 9 unchanged but will make large shifts in the size of the different contributions and therefore only the sum should be interpreted.

2.3. *Isotropically averaged oscillator strengths*

Truncating the expansion of the oscillator strengths in Eq. 9 at the second order gives the dipole and quadrupole intensities. The isotropically averaged oscillator strengths are here written in the length representation since this has been used in the implementation. The zeroth order in Eq. 9 is the electric-dipole-electric-dipole

$f_{0n}^{(\mu^2)}$ contribution

$$\langle f_{0n}^{(\mu^2)} \rangle_{iso} = \frac{2m_e}{3e^2\hbar^2} E_{0n} \sum_{\alpha} \langle 0|\hat{\mu}_\alpha|n\rangle^2 = \frac{2m_e}{3e^2\hbar^2} E_{0n} \langle 0|\hat{\boldsymbol{\mu}}|n\rangle^2 \tag{12}$$

where the sum is over x, y, z if Cartesian coordinates is used. The first order in Eq. 9 vanishes, since the real term is zero, while the second order gives four non-zero contributions. The electric-quadrupole-electric-quadrupole $f_{0n}^{(Q^2)}$ contribution

$$\langle f_{0n}^{(Q^2)} \rangle_{iso} = \frac{m_e}{20e^2\hbar^4c^2} E_{0n}^3 \left[\sum_{\alpha\beta} \langle 0|\hat{Q}_{\alpha\beta}|n\rangle^2 - \frac{1}{3} (\sum_{\alpha} \langle 0|\hat{Q}_{\alpha\alpha}|n\rangle)^2 \right] \tag{13}$$

along with the magnetic-dipole-magnetic-dipole $f_{0n}^{(m^2)}$

$$\langle f_{0n}^{(m^2)} \rangle_{iso} = \frac{2m_e}{3e^2\hbar^2} E_{0n} \sum_{\alpha} \langle 0|\hat{m}_\alpha|n\rangle^2 = \frac{2m_e}{3e^2\hbar^2} E_{0n} \langle 0|\hat{\boldsymbol{m}}|n\rangle^2 \tag{14}$$

are the two terms normally included when the order expansion is truncated at the first order in the transition moments in Eq. 10. The isotropic average of the electric-quadrupole-magnetic-dipole $f_{0n}^{(Qm)}$ contibution is zero.

Since neither $f_{0n}^{(Q^2)}$, $f_{0n}^{(m^2)}$ or the sum of these contributions are origin independent, as discussed in Sec. 2.4, means that only including the $f_{0n}^{(Q^2)}$ and $f_{0n}^{(m^2)}$ as second order terms will become problematic in oxo-bridged multi-metal systems and other systems where there is more than one scattering center and where there is significant $f_{0n}^{(\mu^2)}$ contribution as discussed in Sec. 1. These problems will also be discussed in more detail in Sec. 2.4 where the origin dependence of the transition moments is repeated.

To achieve origin independence the electric-dipole-electric-octupole $f_{0n}^{(\mu O)}$ contribution

$$\langle f_{0n}^{(\mu O)} \rangle_{iso} = -\frac{2m_e}{45e^2\hbar^4c^2} E_{0n}^3 \sum_{\alpha\beta} \langle 0|\hat{\mu}_\beta|n\rangle \langle 0|\hat{O}_{\alpha\alpha\beta}|n\rangle \tag{15}$$

along with the electric-dipole-magnetic-quadrupole $f_{0n}^{(\mu\mathcal{M})}$ contribution

$$\langle f_{0n}^{(\mu\mathcal{M})} \rangle_{iso} = \frac{m_e}{3e^2\hbar^3c} E_{0n}^2 \sum_{\alpha\beta\gamma} \varepsilon_{\alpha\beta\gamma} \langle 0|\hat{\mu}_\beta|n\rangle Im\langle 0|\hat{\mathcal{M}}_{\gamma\alpha}|n\rangle \tag{16}$$

have to be included since these terms are also of the second order expansion of the oscillator strengths.

2.4. *Origin dependence of the transition moments*

As shown in [22] the individual terms in the expansion of the oscillator strengths in Eqs. 13-16 are not origin independent, except the electric-dipole-electric-dipole term, but rely on exact cancellation for the total oscillator strength order for order. To assess when problems in conserving origin independence can occur numerically it is interesting to examine what happens to the individual transition moments

when the origin is shifted from $\boldsymbol{O}$ to $\boldsymbol{O}+\boldsymbol{a}$. For the electric-quadrupole transition moments

$$\langle 0|\hat{Q}_{\alpha\beta}(\boldsymbol{O}+\boldsymbol{a})|n\rangle = \langle 0|\hat{Q}_{\alpha\beta}(\boldsymbol{O})|n\rangle - a_\beta\langle 0|\hat{\mu}_\alpha|n\rangle - a_\alpha\langle 0|\hat{\mu}_\beta|n\rangle, \tag{17}$$

where the α,β are the different x,y,z components, the electric-octupole transition moments

$$\begin{aligned}\langle 0|\hat{O}_{\alpha\alpha\beta}(\boldsymbol{O}+\boldsymbol{a})|n\rangle = &\langle 0|\hat{O}_{\alpha\alpha\beta}(\boldsymbol{O})|n\rangle \\ &- a_\gamma\langle 0|\hat{Q}_{\alpha\beta}(\boldsymbol{O})|n\rangle - a_\beta\langle 0|\hat{Q}_{\alpha\gamma}(\boldsymbol{O})|n\rangle - a_\alpha\langle 0|\hat{Q}_{\beta\gamma}(\boldsymbol{O})|n\rangle \\ &+ a_\alpha a_\beta\langle 0|\hat{\mu}_\gamma|n\rangle + a_\alpha a_\gamma\langle 0|\hat{\mu}_\beta|n\rangle + a_\beta a_\gamma\langle 0|\hat{\mu}_\alpha|n\rangle,\end{aligned} \tag{18}$$

the magnetic-dipole transition moments

$$\begin{aligned}\langle 0|\hat{m}_\alpha(\boldsymbol{O}+\boldsymbol{a})|n\rangle &= \langle 0|\hat{m}_\alpha(\boldsymbol{O})|n\rangle - \varepsilon_{\alpha\beta\gamma}a_\beta\frac{1}{2c}\langle 0|\hat{\mu}^p_\gamma|n\rangle \\ &= \langle 0|\hat{m}_\alpha(\boldsymbol{O})|n\rangle - \varepsilon_{\alpha\beta\gamma}a_\beta\frac{\imath E_{0n}}{2\hbar c}\langle 0|\hat{\mu}_\gamma|n\rangle,\end{aligned} \tag{19}$$

where $\varepsilon_{\alpha\beta\gamma}$ is the Levi-Civita tensor, and the magnetic-quadrupole transition moments

$$\begin{aligned}\langle 0|\hat{\mathcal{M}}_{\gamma\alpha}(\boldsymbol{O}+\boldsymbol{a})|n\rangle = &\langle 0|\hat{\mathcal{M}}_{\gamma\alpha}(\boldsymbol{O})|n\rangle \\ &- \frac{1}{3c}\varepsilon_{\alpha\gamma\delta}a_\gamma\langle 0|\hat{Q}^p_{\beta\delta}(\boldsymbol{O})|n\rangle + \frac{2}{3c}\varepsilon_{\alpha\gamma\delta}a_\beta a_\gamma\langle 0|\hat{\mu}^p_\delta|n\rangle \\ &+ \frac{2}{3}\delta_{\alpha\beta}(\boldsymbol{a}\cdot\langle 0|\hat{\boldsymbol{m}}(\boldsymbol{O})|n\rangle - 2a_\beta\langle 0|\hat{m}_\alpha(\boldsymbol{O})|n\rangle \\ &= \langle 0|\hat{\mathcal{M}}_{\gamma\alpha}(\boldsymbol{O})|n\rangle \\ &+ \frac{\imath E_{0n}}{3\hbar c}\varepsilon_{\alpha\gamma\delta}a_\gamma\langle 0|\hat{Q}_{\beta\delta}(\boldsymbol{O})|n\rangle - \frac{\imath 2E_{0n}}{3\hbar c}\varepsilon_{\alpha\gamma\delta}a_\beta a_\gamma\langle 0|\hat{\mu}_\delta|n\rangle \\ &+ \frac{2}{3}\delta_{\alpha\beta}(\boldsymbol{a}\cdot\langle 0|\hat{\boldsymbol{m}}(\boldsymbol{O})|n\rangle - 2a_\beta\langle 0|\hat{m}_\alpha(\boldsymbol{O})|n\rangle\end{aligned} \tag{20}$$

where the terms electric-dipole μ^p_δ and electric-quadrupole terms $\hat{Q}^p_{\beta\delta}$ have been converted from the velocity to the length representation.

The shifting of the origin in Eqs. 17-20 all produce all lower order contributions. This means that the shift will introduce a linear distance dependence of the electric-dipole transition moments on the electric-quadrupole and magnetic dipole transistion moments and for the electric-octupole and magnetic-quadrupole transition moments the distance dependence of the electric-dipole transition moments will be quadratic. The distance dependence of the transition moments will have multiple effects in molecules with multiple scattering centers. If the electric-dipole transition moments are non-zero then for transitions, which for symmetry reasons will have identical total oscillator strengths, will have different individual contributions to the total oscillator strengths and there need not exist a single coordinate system where a symmetry between the different contributions can be restored. Furthermore, the total oscillator strengths for transitions, which for symmetry reasons will have identical total oscillator strengths, will also be different unless the commmutation relations, in the conversion from the velocity to the length representation, are exactly fullfilled since the order by order cancellation depends on this. If the

total oscillator strengths is not conserved the difference between transitions, which for symmetry reasons will have identical total oscillator strengths, will depend on where the coordinate is placed. This exact problems is faced in oxo-bridged multi-metal systems, in the length representation, since significant electric-dipole transition moments occur in otherwise dipole forbidden transitions due to orbital mixing with the ligands.

For the magnetic-dipole and magnetic-quadrupole transition moments in Eqs. 19 and 20, respectively, the electric-dipole transition moments have been converted from the velocity to the length representation. The magnetic-dipole and magnetic-quadrupole transition moments will therefore only show approximate origin dependence if the conversion form the velocity to the length representation is not exact. The electric-quadrupole and electric-octupole transition moments in Eqs. 17 and 18 will, however, show exact origin dependence both the velocity and length representation. Rewriting the electric-quadrupole and electric-octupole transition moments to the velocity representation is simple. For the electric-quadrupole transition moments

$$\langle 0|\hat{Q}^p_{\alpha\beta}(\boldsymbol{O}+\boldsymbol{a})|n\rangle = \langle 0|\hat{Q}^p_{\alpha\beta}(\boldsymbol{O})|n\rangle - a_\beta\langle 0|\hat{\mu}^p_\alpha|n\rangle - a_\alpha\langle 0|\hat{\mu}^p_\beta|n\rangle \tag{21}$$

and electric-octupole transition moments

$$\begin{aligned}\langle 0|\hat{O}^p_{\alpha\alpha\beta}(\boldsymbol{O}+\boldsymbol{a})|n\rangle = {} & \langle 0|\hat{O}^p_{\alpha\alpha\beta}(\boldsymbol{O})|n\rangle \\ & - a_\gamma\langle 0|\hat{Q}^p_{\alpha\beta}(\boldsymbol{O})|n\rangle - a_\beta\langle 0|\hat{Q}^p_{\alpha\gamma}(\boldsymbol{O})|n\rangle - a_\alpha\langle 0|\hat{Q}^p_{\beta\gamma}(\boldsymbol{O})|n\rangle \\ & + a_\alpha a_\beta\langle 0|\hat{\mu}^p_\gamma|n\rangle + a_\alpha a_\gamma\langle 0|\hat{\mu}^p_\beta|n\rangle + a_\beta a_\gamma\langle 0|\hat{\mu}^p_\alpha|n\rangle\end{aligned} \tag{22}$$

in the velocity representation all terms now just come in the velocity representation just like all terms in the length representation came out in the length representation. The origin dependence of the electric-quadrupole and electric-octupole are therefore trivially reproduced in any basis, representation or level of wavefunction theory [25].

We have used the exact origin dependence to verify the correctness of our implementation of the $f^{(Q^2)}_{0n}$ and $f^{(\mu O)}_{0n}$. The origin dependence in the length representation have for small systems been used to verify the correctness of the implementation for the $f^{(m^2)}_{0n}$ and $f^{(\mu\mathcal{M})}_{0n}$ where the basis set could increased to up largest basis sets available and the exact origin dependence of the $f^{(m^2)}_{0n}$ was checked with the electric-dipole transition in the velocity representation. Like in benchmark studies of molecular properties [28–30] the inclusion of diffuse functions is here also very important to show the origin dependence of the $f^{(m^2)}_{0n}$ and $f^{(\mu\mathcal{M})}_{0n}$ oscillator strengths in the length representation and in general for converging the different contributions.

3. Implementation and computational details

The RASSCF calculations were performed as state-average calculations with the 1s orbitals in RAS1, allowing up to one excitation and with the valence orbitals in RAS2. Orbitals were obtained separately for ground and core-excited states. For the calculations of the excited states, the weights of all configurations with a doubly occupied 1s orbital have been set to zero. The method to relax core holes published by Jensen and Ågren,[9] is not compatible with the current optimization algorithm in the MOLCAS program package [31]. To avoid orbital rotation, i.e.,

that the hole variationally collapses to higher-energy orbital, the $1s$ orbital was frozen in the optimizations of the final states.

Oscillator strengths between the non-orthogonal states were calculated using the biorthonormalization approach in the RASSI program. [32, 33] This procedure removes the problems associated with the use of non-orthogonal states such as gauge dependence. Due to relatively weak spin-orbit coupling, all excited states have the same spin multiplicity as the ground state. A second-order Douglas-Kroll-Hess Hamiltonian with an associated relativistic atomic natural orbital basis set was used to take into account the scalar relativistic effects.[34–37] A density-fitting approximation of the electron repulsion integrals was used to reduce the cost of the calculations, especially important for the large iron dimer.[38]

The origin-independent quadrupole oscillator strengths, as shown in Eqs. 13-16, have been implemented in the RASSI module of the MOLCAS program package. The integrals for the electric part of the multipole expansion, in the length representation, and for the angular momentum operator was already available in the MOLCAS program package [31]. Since the integrals for the electric parts in the length representation already were available and since the length representation is usually used in quantum chemistry, at least for the dipole, we have chosen to examine if the length representation also will be applicapable for intensities beyond the dipole. The integral code was therefore extended with the integrals for the spin-independent orbital magnetic-quadrupole operator:

$$\hat{\mathcal{M}}_{\alpha\beta} = \frac{e}{2m_e c} \sum_i \frac{2}{3} (r_{i,\beta}(\boldsymbol{r}_i \times \hat{\boldsymbol{p}}_i)_\alpha + (\boldsymbol{r}_i \times \hat{\boldsymbol{p}}_i)_\alpha r_{i,\beta}). \tag{23}$$

The integrals are evaluated using a Hermite-Gauss quadrature.

The correctness of the implementation has been verified by explicitly programming the origin dependence of every term as mentioned in Sec. 2.4. The origin-independent quadrupole intensities code will be released with the next MOLCAS release.

For the Fe^{3+} atomic system only the 3d orbitals are included in the RAS2 space. This d^5 system has high-spin ^{6}S ground state with one electron in each orbital, from which there are only five possible core excited states. $[FeCl_4]^{1-}$ has a T_d geometry with an Fe-Cl distance of 2.186 Å. [39] The RAS2 space has 11 electrons in 13 orbitals, see Figure 1, and the orbitals of the sextet excited states were averaged over 70 states.

The geometry of [(hedta)FeOFe(hedta)] was obtained from a BP86/6-311(d) geometry optimization. This give an Fe-O distance of 1.76 Å and an Fe-O-Fe angle of 148 degrees, see Figure 2. The structure of the three-atom model Fe-O-Fe complex were extracted from the full complex. The RAS2 space for these systems consists of the three 2p orbitals of the bridging oxygen and the ten 3d orbitals of the irons, which gives a total of 16 electrons in 13 valence orbitals, see Figure 1.

For both the iron dimers the ground state of the is an antiferromagnetically coupled singlet, with five unpaired electrons on each iron. To achieve stable RASSCF convergence, calculations are instead performed with ferromagnetic coupling between iron, giving undectet states. For the Fe-O-Fe model, 60 core-excited states were used while for [(hedta)FeOFe(hedta)] all possible 1716 undectet states were included.

To be able to freely move the origin in the simulations, calculations have been performed without the use of symmetry. The exception is the full hedta dimer where the correct C_2 symmetry was used.

Experimental K-edge spectra are taken from reference [1]. Simulated spec-

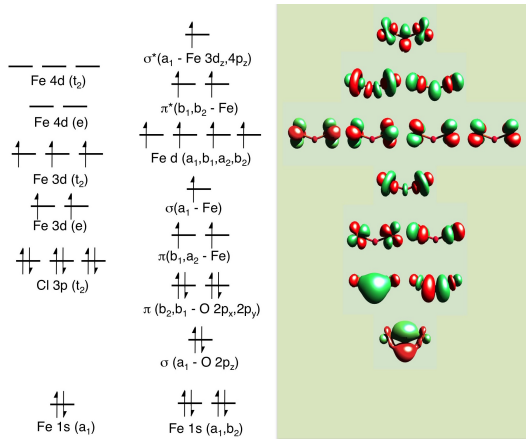

Figure 1. Active orbital diagrams for $[FeCl_4]^{1-}$ (left) and Fe_2O (middle). For Fe_2O the shapes of the active orbitals are also shown (right).

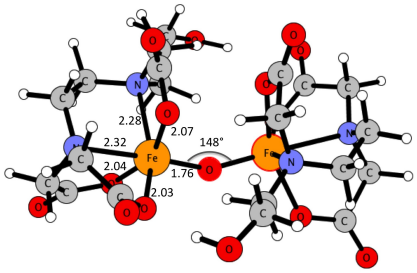

Figure 2. Geometric structure of the [(hedta)FeOFe(hedta)] complex.

tra are plotted using a Lorentzian lifetime broadening with a full-width-at-half-maximum (FWHM) of 1.25 eV and further convoluted with a Gaussian experimental broadening of 1.06 eV. The incident energy of the calculated spectra for the [(hedta)FeOFe(hedta)] complex are shifted to align with the experimental ones at the first intense transition, which requires a shift of approximately 20 eV where the necessity shift is mainly due to the frozen core approximation. The intensity of the [(hedta)FeOFe(hedta)] spectrum is multiplied by a factor of 1942.5. This is the scaling factor that gave the best fit between calculated and edge-subtracted normalized K-edge intensities in the previous RAS studies, but here divided by two to take into adjust for the presence of two absorption centers.[21]

4. Application

Three distinct x-ray spectroscopy applications of Fe have been chosen to show how the origin independence of the oscillator strengths are affected by the basis set, choice of origin, spin-orbit coupling and multiple scattering centers. The $1s - 3d$ transitions studied here are formally dipole forbidden, however, orbital mixing with the ligands can give significant $f_{0n}^{(\mu^2)}$ contributions to the oscillator strengths otherwise known as pre-edge enhancement. For the basis set part we will here limit ourselves to only discussing the origin independence and not the convergence of the actual oscillator strengths. In the small correlation consistent basis sets some numerical problems are evident. We have chosen to include the results from these basis sets despite not knowing the exact cause of the problem.

We will here discuss basis set effects and how far out the origin independence is numerically conserved simply by moving the origin. Here we will look at individual

intensities and follow these to show how exact the cancellation of the individual contributions is. Both transitions that should be strictly dipole forbidden and transitions with strong dipole contributions are included to show the difference. We will compute spectra for different origins and show how the spectrum is built from the individual terms with different origin dependence. Since the spectra for calculations with and without spin-orbit coupling are almost identical we will not always show both.

4.1. Fe^{3+}

The Fe^{3+} atom is a d^5 system with a ^6S ground state. From there, a quadrupole excitation leads to a ^6D 1s core-excited state. This transition is electric-dipole forbidden, and the $f_{0n}^{(Q^2)}$ and $f_{0n}^{(m^2)}$ contributions, in Eqs 17 and 19, to the total oscillator strength should be constant when the origin is moved, at least in the ideal case. The $f_{0n}^{(\mu O)}$ and $f_{0n}^{(\mu\mathcal{M})}$ contributions, in Eqs 18 and 20 will show distance dependence in the transition moments of the electric octupole and magnetic quadrupole but since the electric dipole, in the ideal case, is zero $f_{0n}^{(\mu O)}$ and $f_{0n}^{(\mu\mathcal{M})}$ should also be origin independent and hence no cancellation would be necessary.

In Figure 3 the origin dependence, in the ANO-RCC-VDZP basis, of the different contributions to the total intensity of the transition from the ground state to the first core-excited state (1s→3d excitation) is shown. As expected, the total intensity is completely dominated by the $f_{0n}^{(Q^2)}$ contribution.

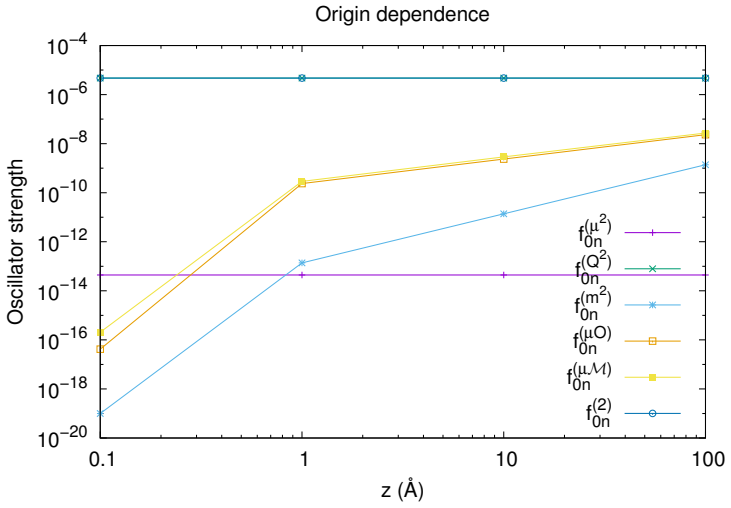

Figure 3. The origin dependence of the different contributions to the total oscillator strength for the transition from the ground state to the first core-excited state in Fe^{3+} in the ANO-RCC-VDZP basis. The origin has been moved to $0.1\mathring{A}$ to fit in the plot. Since the transition shown is dipole forbidden the magnitude of the $f_{0n}^{(\mu O)}$ and $f_{0n}^{(\mu\mathcal{M})}$ intensities grows quadratically with the displacement of the origin along the $z-$axis as would be expected from Eqs. 18 and 20. Since the $f_{0n}^{(\mu^2)}$ intensity is not exactly zero in the calculation the $f_{0n}^{(m^2)}$ intensity also grows with distance. The change in the intensity for the $f_{0n}^{(Q^2)}$ intensity is so small compared to the value at the origin that the change is not visible. Values below 10^{-19} are set to 10^{-19}.

Since the $f_{0n}^{(\mu^2)}$ intensity is not exactly zero for the ANO-RCC-VDZP basis, as seen in Figure 3, then this is not the ideal case and $f_{0n}^{(Q^2)}$, $f_{0n}^{(m^2)}$, $f_{0n}^{(\mu O)}$ and $f_{0n}^{(\mu\mathcal{M})}$ are not constant when the origin is moved. In fact, the ideal behaviour is not observed in any of the basis sets listed in Table 1 and despite $f_{0n}^{(\mu^2)}$ being very small the effect of a non-zero $f_{0n}^{(\mu^2)}$ is very visible.

Basis	$f_{0n}^{(\mu^2)}$	$f_{0n}^{(\mu^2)^p}$	R_{dip}	$f_{0n}^{(2)}$
ANO-RCC-MB				0.354E-05
ANO-RCC-VDZP	0.441E-13	0.456E-13	0.968	0.472E-05
ANO-RCC-VTZP	0.109E-14	0.104E-14	1.051	0.477E-05
ANO-RCC-VQZP	0.225E-12	0.218E-12	1.032	0.463E-05
cc-pVDZ				0.613E-05
AUG-cc-pVDZ	0.560E-15	0.260E-17	215.5	0.265E-04

Table 1. The total dipole- ($f_{0n}^{(\mu^2)}$) and quadrupole ($f_{0n}^{(2)}$) intensities for the transition from the ground state to the first core excited state in Fe^{3+} in the ANO-RCC-VDZP basis set along with the ratio between the dipole intensities R_{dip} defined as $f_{0n}^{(\mu^2)}/f_{0n}^{(\mu^2)^p}$. Values below 10^{-19} is not included.

Since the origin independence is only guaranteed in the velocity representation and because the main error in preserving origin independence comes from the dipole contribution, R_{dip} has therefore been defined as the ratio of the dipole oscillator strength in the length and velocity representation

$$\Delta = f_{0n}^{(\mu^2)^p} - f_{0n}^{(\mu^2)} = f_{0n}^{(\mu^2)^p}(1 - \frac{f_{0n}^{(\mu^2)}}{f_{0n}^{(\mu^2)^p}}) = f_{0n}^{(\mu^2)^p}(1 - R_{dip}) \tag{24}$$

where Δ is the difference between the dipole oscillator strengths in the two representations. From Eq. 24 it is evident that if R_{dip} deviates even slightly from unity, origin dependence will be difficult to preserve in the length representation. This problem is of course more critical if $f_{0n}^{(\mu^2)^p}$ is large.

Looking at different basis sets, the dominating $f_{0n}^{(2)}$ term only changes very little for the ANO-RCC basis sets, see Table 1. However, changing to a correlation consistent basis set gives a large change and when adding diffuse functions the total intensity is almost trebled compared to the ANO-RCC basis sets. The importance of the inclusion of diffuse functions for molecular properties has been demonstrated several times before in the literature [28–30]. R_{dip}, however, grows dramatically going from the ANO-RCC basis sets to the AUG-cc-pVDZ which makes the AUG-cc-pVDZ the basis set with the poorest conservation of origin independence, despite having smaller dipole oscillator strength than the ANO basis sets, as shown in Fig. 4(a). The exact reason for the poor performance of the AUG-cc-pVDZ basis set have not been analyzed.

Despite the non-ideal behaviour a small cancellation of the individual contributions from moving the origin is observed in all basis sets. A complete origin independence is, however, not observed for any of the basis sets. The deviation in $f_{0n}^{(2)}$ from the origin for all basis sets is shown in Fig. 4(a). The changes in $f_{0n}^{(2)}$ are several magnitudes smaller than the $f_{0n}^{(2)}$ values in Table 1, as well as the uncertainty of $f_{0n}^{(2)}$ with respect to the choice of basis set.

Even though the changes in $f_{0n}^{(2)}$ are many magnitudes smaller than the value of $f_{0n}^{(2)}$, cancellation is still taking place as seen by comparing the changes in $f_{0n}^{(Q^2)}$ in Fig. 4(b) with the changes in $f_{0n}^{(2)}$ in Fig. 4(a). These cancellations reduce the change in $f_{0n}^{(2)}$ by one to two magnitudes.

The largest cancellation between the different terms are seen for basis sets where R_{dip}, shown in Table 1, are closest to one. In the ANO-RCC-VTZP basis, where R_{dip} is 1.05, the cancellation is around two orders of magnitude while for the AUG-cc-pVDZ basis, where the ratio is 215.6, practically no cancellation is taking place. The cancellation can be seen by comparing the origin dependence of $f_{0n}^{(2)}$ in Fig. 4(a) and $f_{0n}^{(Q^2)}$ in Fig. 4(b). Hence to ensure good origin independence in the

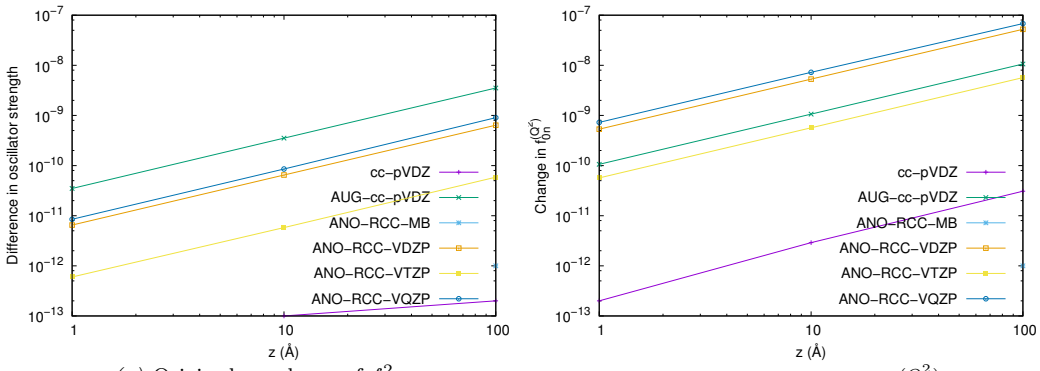

(a) Origin dependence of f_{0n}^2. *(b)* Origin dependence of $f_{0n}^{(Q^2)}$.

Figure 4. The origin dependence of f_{0n}^2 and $f_{0n}^{(Q^2)}$ in the different basis sets shown in Table 1. The origin dependence of f_{0n}^2 and $f_{0n}^{(Q^2)}$ is defined as $|f_{0n}^2(\boldsymbol{O}) - f_{0n}^2(\boldsymbol{O}+\boldsymbol{z})|$ and $|f_{0n}^{(Q^2)}(\boldsymbol{O}) - f_{0n}^{(Q^2)}(\boldsymbol{O}+\boldsymbol{z})|$, respectively.

length representation for transitions with large $f_{0n}^{(\mu^2)}$ contribution, the commutation relations between the approximate Hamiltonian and r must be very accurate since this will determine the ratio between $f_{0n}^{(\mu^2)}$ and $f_{0n}^{(\mu^2)^p}$ [25].

4.2. $[FeCl_4]^{1-}$

As mentioned in Sec. 1, breaking the centrosymmetry can lead to a significant increases in pre-edge intensity through 4p mixing.[1, 2] $[FeCl_4]^{1-}$ is a highly symmetric (T_d) complex, but lack an inversion center. The experimental K pre-edge spectrum of $[FeCl_4]^{1-}$ has a single intense peak at 7113.2 eV. The estimated dipole to quadrupole ratio is 3.2:1.0 and the intensity increases 5.2 times compared to hexa-coordinated $[FeCl_6]^{3-}$ complex.[1]

$[FeCl_4]^{1-}$ has an $e^2t_2{}^3$ electronic configuration and a ${}^6A_1$ ground state. There are two different sets of single-electron core to valence excitations, leading to the configurations, $1s^1e^3t_2{}^3$ and $1s^1e^2t_2{}^4$, giving ${}^6E$ and ${}^6T_2$ excited states. The spectrum is completely dominated by t_2 excitation as it gets dipole contributions from the mixing with $4p$ orbitals (t_2 symmetry).[40]

We will here analyze two transitions between spin-free states with very different electric dipole oscillator strengths. Including spin-orbit coupling merely distributes the intensity over many more transitions and does not alter R_{dip} or the spectrum in any significant way. The transition to the first core-excited state is an e excitation, which ideally should should have zero electric dipole intensity. The transition to the third core excited state is an electric-dipole allowed t_2 excitation.

The dipole and quadrupole intensity for the transition from the ground state to the first core-excited state are shown in Table 2. As was the case for the ion, the dipole intensities are not zero but for the ANO-RCC basis sets the dipole intensities are very small and many magnitudes smaller than the quadrupole intensities, thereby showing that for this transition there is no enhancement of the pre-edge from the 4p mixing. The correlation consistent basis sets, however, gives a dipole intensities only one magnitude smaller than the quadrupole intensity. Unlike the ANO-RCC basis sets the correlation consistent basis sets also have a very large R_{dip} thereby making it impossible to use these basis sets for this problem. For the ANO-RCC basis sets the quadrupole intensity is completely dominated by $f_{0n}^{(Q^2)}$ while for the correlation consistent basis sets $f_{0n}^{(\mu O)}$ gives a contribution of the same magnitude as $f_{0n}^{(Q^2)}$.

Basis	$f_{0n}^{(\mu^2)}$	$f_{0n}^{(\mu^2)^p}$	R_{dip}	$f_{0n}^{(2)}$
ANO-RCC-MB	0.244E-10	0.239E-10	1.024	0.200E-05
ANO-RCC-VDZP	0.300E-12	0.290E-12	1.035	0.394E-05
ANO-RCC-VTZP	0.160E-12	0.149E-12	1.071	0.407E-05
ANO-RCC-VQZP	0.509E-13	0.504E-13	1.009	0.422E-05
cc-pVDZ	0.816E-07	0.248E-08	32.93	0.498E-06
AUG-cc-pVDZ	0.765E-06	0.447E-06	1.713	0.258E-05

Table 2. The total dipole- and quadrupole intensities for the transition from the ground to the first core-excited state ($1s \rightarrow e$) in $[FeCl_4]^{1-}$ without spin-orbit coupling.

Basis	$f_{0n}^{(\mu^2)}$	$f_{0n}^{(\mu^2)^p}$	R_{dip}	$f_{0n}^{(2)}$
ANO-RCC-MB	0.115E-04	0.111E-04	1.040	0.717E-06
ANO-RCC-VDZP	0.295E-04	0.286E-04	1.033	0.116E-05
ANO-RCC-VTZP	0.283E-04	0.273E-04	1.033	0.144E-05
ANO-RCC-VQZP	0.285E-04	0.276E-04	1.033	0.161E-05
cc-pVDZ	0.214E-04	0.198E-04	1.080	-0.530E-04
AUG-cc-pVDZ	0.281E-04	0.168E-04	1.677	-0.585E-04

Table 3. The total dipole- and quadrupole intensities for the transition from the ground to the third core-excited state ($1s \rightarrow t_2$) in $[FeCl_4]^{1-}$ without spin-orbit coupling.

Since $f_{0n}^{(\mu^2)}$ is very small for the $1s \rightarrow e$ excitation in $[FeCl_4]^{1-}$, the change in $f_{0n}^{(2)}$ when the origin is moved is very small, only 10^{-9} between the origin and $30\mathring{A}$ as seen in Figure 5.

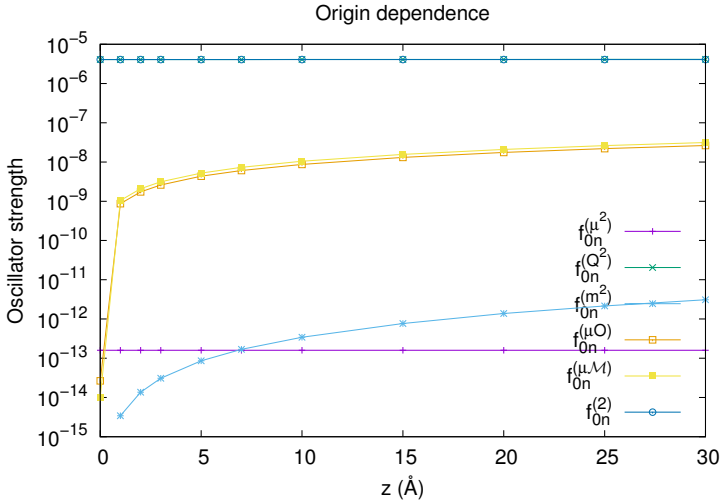

Figure 5. The magnitude of the origin dependence of the different contributions to the total oscillator strength for the transition from the ground state to the first core-excited state in $[FeCl_4]^{1-}$ in the ANO-RCC-VTZP basis without spin-orbit coupling. The electric dipole intensity is very small and the total quadrupole intensity only changes by 10^{-9} between the origin and $30\mathring{A}$.

The dipole and quadrupole intensities for the transitions from the ground to the third core-excited state in different basis are shown in Table 3. For the ANO-RCC basis sets the dipole intensity is approximately 20 times stronger than the quadrupole intensity thereby showing that the 4p mixing can give very significant enhancement of the pre-edge. The correlation consistent basis sets gives a total intensity which is negative and hence physically unacceptable. The negative intensities will be discussed in more detail at the end of this section.

In Table 3 R_{dip} for the ANO-RCC basis sets is 1.03-1.04, which should give a cancellation of the different second order contributions of two magnitudes. This

cancellation in $f_{0n}^{(2)}$ can be seen i Fig. 6, where $f_{0n}^{(2)}$ is approximately two orders of magnitude smaller than all other terms when the origin is moved. This exact trend is seen in all the ANO-RCC basis sets while the correlation consistent basis sets again produce inferior results since R_{dip} is significantly larger. Despite having a cancellation of two orders of magnitude in the ANO-RCC basis sets the different terms, however, grows rapidly with distance, since $f_{0n}^{(\mu^2)}$ is large, and at 7$\mathring{A}$ $f_{0n}^{(2)}$ is larger than $f_{0n}^{(\mu^2)}$. It is therefore evident that for transitions where $f_{0n}^{(\mu^2)}$ is large, the range where $f_{0n}^{(2)}$ can safely be calculated, in the length representation, is limited. The range can, however, be reasonably estimated from R_{dip} and $f_{0n}^{(\mu^2)^p}$ since R_{dip} gives information about the cancellation and $f_{0n}^{(\mu^2)^p}$ about the growth of the different terms.

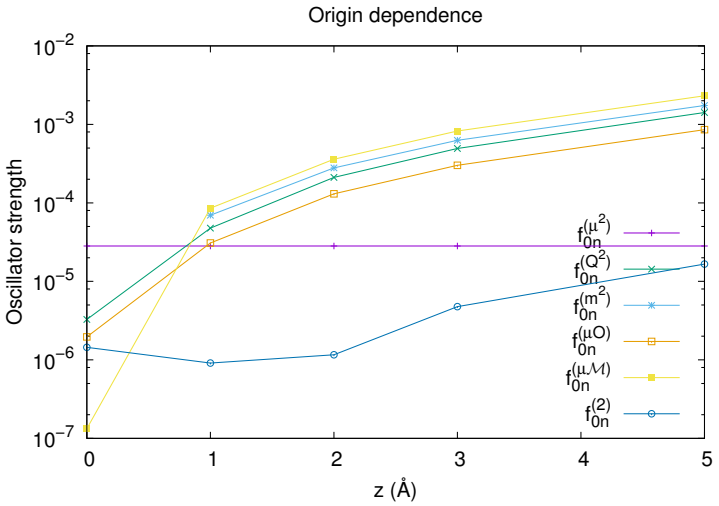

Figure 6. The magnitude of the origin dependence of the different contributions to the total oscillator strength for the transition from the ground state to the third core-excited state in $[FeCl_4]^{1-}$ in the ANO-RCC-TZVP basis without spin-orbit coupling. When the origin is moved along the z-direction the individual contributions rapidly rise by three to five magnitudes. There is thoughout a cancellation of approximately two magnitudes when comparing the total to the individual terms. At about 7.0 $\mathring{A}$ the error in the total quadrupole intensity is larger than the dipole intensity.

R_{dip} is, however, not the same for all transitions which can be seen by comparing R_{dip} for the transition from the ground state to the first core-excited state in Table 2 with R_{dip} for the transition from the ground state to the third core-excited state in Table 3. While the ANO-RCC basis sets produce similar R_{dip} for the two different transitions the correlation consistent basis sets produce very different R_{dip}.

By comparing Fig. 5 and Fig. 6 it is evident that conserving the origin independence for transitions with large $f_{0n}^{(\mu^2)}$ is significantly more difficult than for transitions with small $f_{0n}^{(\mu^2)}$. Since not all intensities is shifted equally when the origin is moved the spectrum will also change when the origin is moved, this, however, need not be visible to the eye.

The unshifted spectrum for $[FeCl_4]^{1-}$ with Fe in the origin in the ANO-RCC basis as shown in Fig. 7 compare very well with previous publications on calculations on $[FeCl_4]^{1-}$ [21] except in the minimal basis. The shape and the intensity of the spectrum, when spin-orbit coupling is included, only shows minor changes going from the ANO-RCC-VDZP basis to the ANO-RCC-VQZP basis and practically no change when spin-orbit coupling is excluded since the ANO-RCC-VQZP and spin-free (SF)-ANO-RCC-VQZP spectra are right on top of each other. The spectrum is, however, shifted significantly towards the experimental spectrum, where

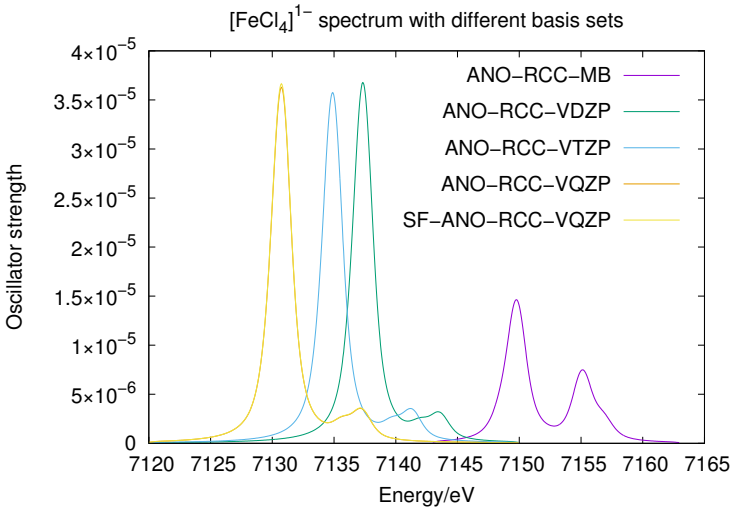

Figure 7. The unshifted spectrum of $[FeCl_4]^{1-}$ in different ANO-RCC basis sets with spin-orbit coupling included except for the SF-ANO-RCC-VQZP calculation. The spectra are plotted using a Lorentzian broadening with a full-width-at-half-maximum (FWHM) of 1.25 eV and further convoluted with a Gaussian broadening of 1.06 eV [21, 41].

the main peak in the experiment is at 7113.2 eV [1], when the basis set is increased.

By moving the origin from the Iron atom and along the $z-$direction the change in the shape of the spectrum for distances up to $3\mathring{A}$ is minor, see Fig. 8. For a displacement of the origin larger than $3\mathring{A}$ there is a pronounced change in shape and intensity. At $5\mathring{A}$ the intensity is approximately halved, while at $7\mathring{A}$ there is practically no intensity. Finally, at $10\mathring{A}$ the shape of the spectrum is very close to that with Fe in the origin, just with opposite sign for the intensity.

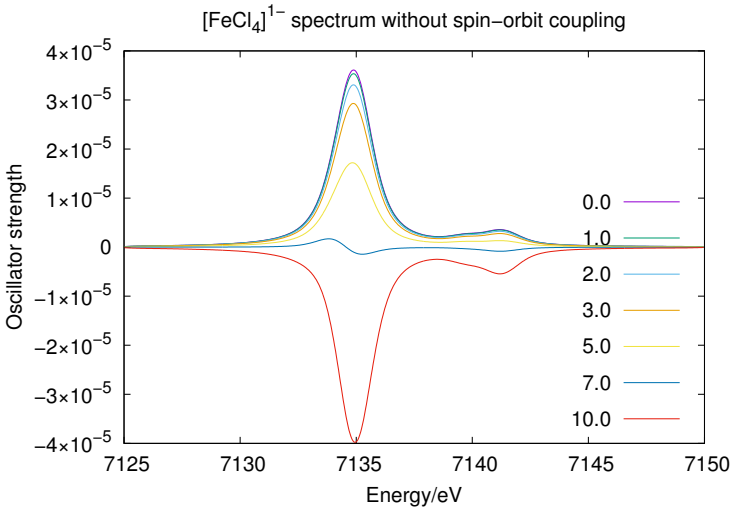

Figure 8. The unshifted spectrum of $[FeCl_4]^{1-}$ in the ANO-RCC-VTZP basis set with an origin displacement along the $z-$axis up to $10\mathring{A}$. Here the shape of the spectrum changes significantly when the origin is moved more than $3\mathring{A}$. At $7\mathring{A}$ the intensity is extremely low while at $10\mathring{A}$ the spectrum has the same shape as for $0\mathring{A}$ but with opposite sign.

The changes in the spectrum in Fig. 8 follow the trend from the change in $f_{0n}^{(2)}$ in Fig. 6 where $f_{0n}^{(2)}$ changes sign and increases in absolute value when the origin is moved away from Fe. At distances up to $3\mathring{A}$ $f_{0n}^{(\mu^2)}$ is still significantly larger than $f_{0n}^{(2)}$ and the change in the spectrum, as seen in Fig. 8, is minor while at $5\mathring{A}$ the absolute

value of $f_{0n}^{(2)}$ start to be comparable with $f_{0n}^{(\mu^2)}$ and the intensity in the spectrum drops significantly. For long distances $f_{0n}^{(2)}$ will give the dominant contribution to the spectrum and therefore give the negative intensity for the spectrum at $10\mathring{A}$. Had the cancellation not changed the sign of $f_{0n}^{(2)}$ there would have been no change in the shape of the spectrum, only in the intensity.

While the change in the spectrum between having Fe in the origin and at $1\mathring{A}$ is hard to discern from Fig. 8, the individual contributions to $f_{0n}^{(2)}$ changes significantly as shown in Fig. 9. The cancellation of the individual contributions in $f_{0n}^{(2)}$ thus have to very good in order to conserve the origin independence since the individual contributions are significantly larger than the total. These large terms have to combine to a $f_{0n}^{(2)}$ that should be give much smaller contributions to the spectrum compared with $f_{0n}^{(\mu^2)}$.

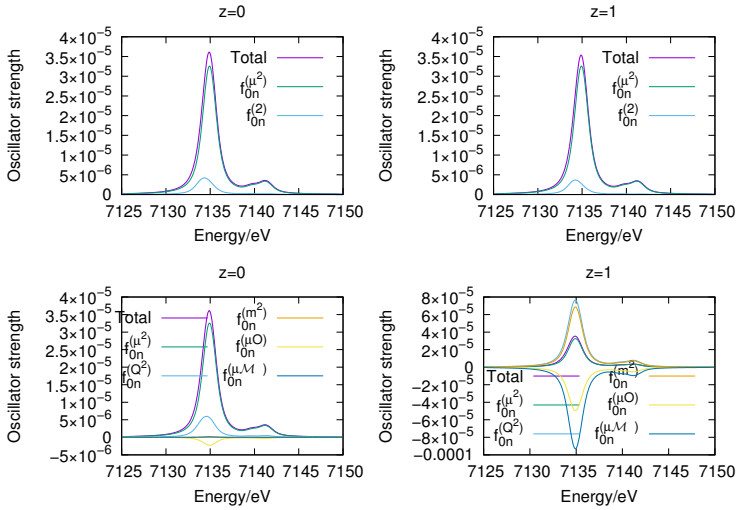

Figure 9. A comparison of the spectrum for $[FeCl_4]^{1-}$ in the ANO-RCC-VTZP basis set at $z = 0\mathring{A}$ and $z = 1\mathring{A}$ where in the first row the $f_{0n}^{(\mu^2)}$ and $f_{0n}^{(2)}$ contributions to the total are plotted. In the second row the individual contributions to $f_{0n}^{(2)}$ are shown.

Negative intensities, with the transition metal in the origin, have been observed before in similar systems [27] where it was attributed to not including higher order terms in the multipole expansion. Since this only happens in certain basis sets, this indicates that this a basis set problem rather than a problem of not including higher orders in Eq. 9. Since all transition moments does not have the same basis set requirement the transition moments can therefore be under- or overestimated independently of each other and hence give total negative intensities for a finite truncation of the multipole expansion. Such an explanation would also be more in line with the usual explanation where $s \rightarrow p$ and $s \rightarrow d$ transitions are dipole and quadrupole allowed, respectively, where the dipole intensity is significantly larger than the quadrupole intensity and enhancements from orbital mixing comes in the lower order contributions.

For the ANO-RCC basis sets the quadrupole intensities are dominated by $f_{0n}^{(Q^2)}$ and $f_{0n}^{(\mu O)}$ where the contribution from $f_{0n}^{(Q^2)}$ is positive and $f_{0n}^{(\mu O)}$ negative. For the correlation consistent basis sets the quadrupole intensities are completely dominated by $f_{0n}^{(\mu O)}$, which are negative. Here again the different basis sets give very different values for $f_{0n}^{(Q^2)}$ and $f_{0n}^{(\mu O)}$, thereby showing the unbalanced treatment in some basis sets and the independent under- or overestimation of the transition mo-

ments. This unbalanced treatment can be seen by comparing the spectra plotted in Fig. 10 using the AUG-cc-pVDZ basis set and Fig. 8 using the ANO-RCC-VTZP basis set. The same number of excited states have been used in both calculations, which shows that many excited states are missing in the AUG-cc-pVDZ calculations. The spectrum in Figure 10 is very negative and could only be remedied by including higher orders in the multipole expansion, here at least to $f_{0n}^{(4)}$ to include $f_{0n}^{(O^2)}$, provided that none of the higher order transition moments will be larger than the electric octopole transition moment. That f_{0n}, in Eq. 9, always will give positive intensities for finite truncation of the multipole expansion in finite basis sets is not clear nor is the convergence behaviour of the multipole expansion.

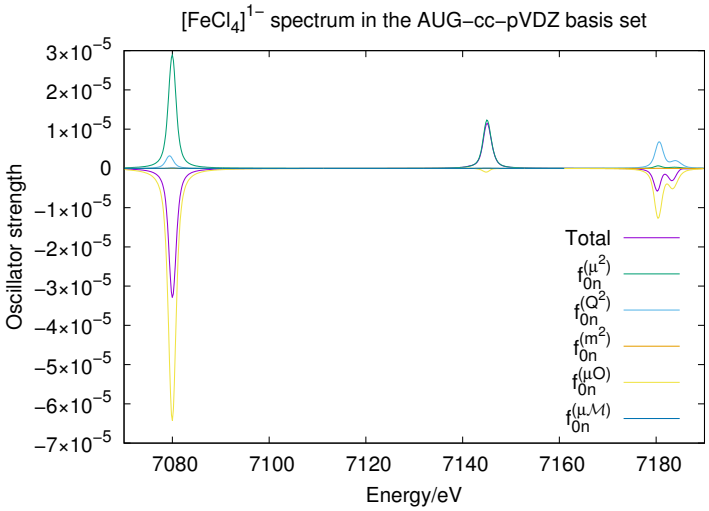

Figure 10. The spectrum for $[FeCl_4]^{1-}$ in the AUG-cc-pVDZ basis with Fe in the origin along with all the individual contributions to $f_{0n}^{(2)}$ is shown.

4.3. *Fe-O-Fe model system and [(hedta)FeOFe(hedta)]*

The μ-oxo-bridged iron dimers have have two high-spin d^5 centers. The ground state has antiferromagnetic coupling, giving an open-shell singlet. The energy difference compared to the ferromagnetically coupled undectet is 0.1 eV, relatively small compared to the range of the K pre-edge. As as the electronic structure of the undectet is significantly simpler, the analysis is made using that structure.

The 13 orbitals in the active space consist of three doubly occupied Fe(3d)-O(p) bonding orbitals, seven singly occupied metal-3d-dominated orbitals and three singly occupied anti-bonding iron-oxygen orbitals, see Figure 1. The Fe-O-Fe core has C_{2v} symmetry and the hedta complex has C_2 symmetry. The individual iron sites can be viewed as having iron C_{4V} symmetry with axial ligand distances in the plane of more than 2.0 Å and a short iron-oxygen bond distance of 1.76 Å, see Figure 2. The distortion away from centrosymmetry leads to mixing of metal 4p orbitals into the valence space and thus the possibility for dipole-allowed transitions in the pre-edge.

4.3.1. Fe-O-Fe

In Sec. 4.2 some problems in keeping the origin independence occured for transitions with large $f_{0n}^{(\mu^2)}$ contributions. Since the distance between the two Fe centers is approximately 3.39 Å it is essential that the origin independence can be safely

Basis	$f_{0n}^{(\mu^2)}$	$f_{0n}^{(\mu^2)^p}$	R_{dip}	$f_{0n}^{(2)}$
ANO-RCC-MB	0.590E-07	0.497E-07	1.189	0.200E-05
ANO-RCC-VDZP	0.540E-07	0.556E-07	0.971	0.168E-05
ANO-RCC-VTZP	0.400E-07	0.408E-07	0.981	0.151E-05
ANO-RCC-VQZP	0.373E-07	0.391E-07	0.954	0.119E-05
cc-pVDZ	0.418E-07	0.411E-07	1.017	0.171E-05
AUG-cc-pVDZ	0.353E-07	0.358E-07	0.985	0.167E-05

Table 4. The total dipole- and quadrupole intensities for the transition from the ground state to the first core-excited state in Fe-O-Fe. In the ANO-RCC-MB basis this is the fifth core-excited state. The strongest $f_{0n}^{(\mu^2)}$ is approximately $0.2E-05$ and hence around the same size as the strongest $f_{0n}^{(2)}$. The origin is here placed in the oxygen atom and 1.76 Å from the iron atoms.

conserved to at least 1.69 Å away from an Fe atom, since the origin then can be placed between the two Fe atoms without any problems. We will, however, initially place the origin on the O atom, since this would be the natural place in C_{2v} symmetry, and then move along the molecular plane perpendicular to the C_2 rotational axis. This direction is usually labeled the y-axis, but here becomes the displacement vector z.

Looking at the size of $f_{0n}^{(\mu^2)}$ and $f_{0n}^{(2)}$ for the first core-excited state in Table 4, it is evident that $f_{0n}^{(2)}$ dominate in the total oscillator strength for the first transitions. However, there does not exist a coordinate system where there will not be a need for exact cancellation to determine the ratio between the $f_{0n}^{(\mu^2)}$ and $f_{0n}^{(2)}$ contributions. The ratio R_{dip} is about the same as for $[FeCl_4]^{1-}$ and Fe^{3+} where a cancellation of up to two magnitudes is observed, hence we do expect that $f_{0n}^{(2)}$ will not be significantly affected by the origin dependendence since $f_{0n}^{(\mu^2)}$ is not significantly larger than $f_{0n}^{(2)}$ for any of the excitations calculated for the spectrum.

With the origin on the oxygen atom, the spectrum shows three distinct peaks, except in the minimum basis, as shown in Fig. 11. Like in the spectrum for $[FeCl_4]^{1-}$ in Fig. 7 there is only minor variations in the shape of the spectra in the different basis sets. The intensity, however, does vary more than for $[FeCl_4]^{1-}$. Again the expected downward shift in the energy when the basis set is increased is observed. Despite the fact that the largest change in intensity is seen going from the ANO-RCC-VTZP to ANO-RCC-VQZP, we will continue the analysis using the ANO-RCC-VTZP since this is a realistically sized basis set when going beyond the model systems.

Spectra with the origin in different places are shown in Fig. 12. Placing the origin on the oxygen atom ($O_{z=0}$), between the iron atoms (Fe-Fe), on one of the iron atoms (Fe) or even moving the origin a bit from the oxygen atom ($O_{z=1}$) does not alter the spectrum. For these kinds of systems we can safely choose between any of the natural choices of origin and the method is therefore also applicable for molecules with multiple heavy centers.

When the origin is moved further away ($O_{z=3}$ and $O_{z=5}$) the total and relative intensity of the three peaks changes. Here the intensity of the large central peak changes significantly more than the two peaks on the side. This can be understood by looking at the spectra for $f_{0n}^{(\mu^2)}$ and $f_{0n}^{(2)}$, where for the central peak the intensity is primarily from $f_{0n}^{(\mu^2)}$ while for the two other peaks the $f_{0n}^{(\mu^2)}$ contribution is significantly smaller. This causes the central peak to be more sensitive to origin displacements as can be seen from Eq. 24. From the spectrum of $f_{0n}^{(\mu^2)}$ and $f_{0n}^{(2)}$ it is also evident that the first peak in fact is two close lying peaks, one from both $f_{0n}^{(\mu^2)}$ and $f_{0n}^{(2)}$, which also explains the apparent broadness of the first peak compared to

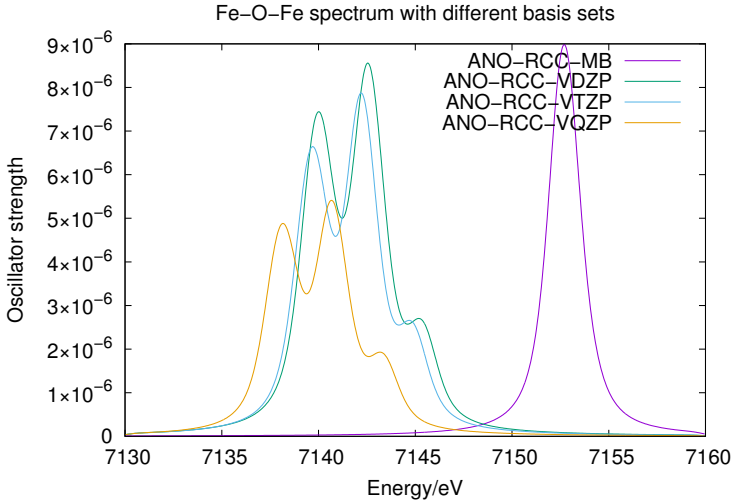

Figure 11. The unshifted spectra of Fe-O-Fe in different ANO-RCC basis sets.

the more intense central peak. Therefore having both $f_{0n}^{(\mu^2)}$ and $f_{0n}^{(2)}$ is central in the understanding of a spectrum since $f_{0n}^{(\mu^2)}$ and $f_{0n}^{(2)}$ will be conserved separately unlike the contributions to $f_{0n}^{(2)}$.

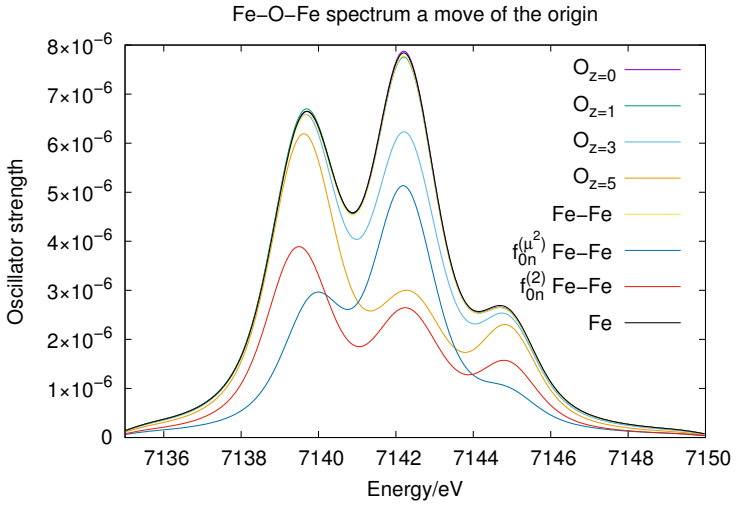

Figure 12. A comparison of the spectra for Fe-O-Fe with the origin in the oxygen atom ($O_{z=0}$), origin moved along the z-axis ($O_{z=d}$), where d is the distance, the origin in the middle between the two Fe atoms (Fe-Fe) and the origin placed on one of the Fe atom (Fe) in the ANO-RCC-VTZP basis set. The $f_{0n}^{(\mu^2)}$ and $f_{0n}^{(2)}$ contributions are shown with the origin placed between the two Fe atoms.

While the spectrum did not change significantly with some of the origin displacements in Fig. 12 the individual terms that sum to $f_{0n}^{(2)}$ do. The change in $f_{0n}^{(Q^2)}$ for the origin displacements, where $f_{0n}^{(2)}$ did not change, have been plotted in Fig. 13. The intensities from $f_{0n}^{(Q^2)}$ is around 6 to 11 times as intensive as compared to the total intensity in Fig. 12 and it is therefore obvious that for molecules with multiple heavy centers all terms in the quadrupole intensities have to be included. Furthermore Fig. 13 also shows that interpreting the individual contributions to $f_{0n}^{(2)}$ does not make sense since these are heavily influenced by the choice of origin.

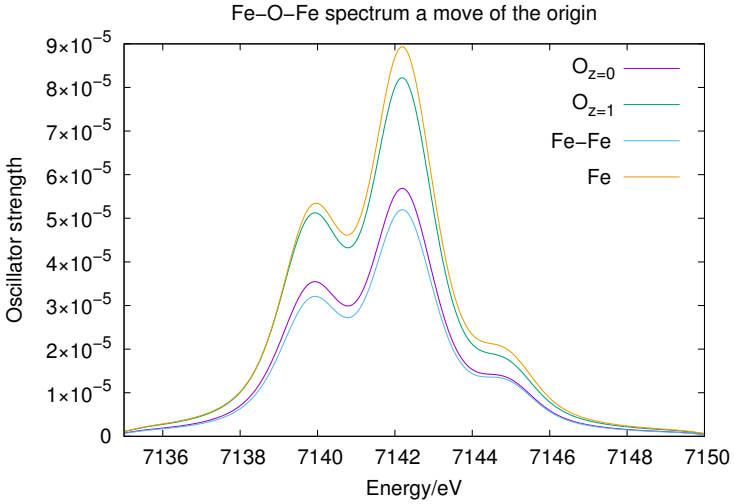

Figure 13. A comparison of the spectra for $f_{0n}^{(Q^2)}$ for Fe-O-Fe with the origin in the Oxygen atom ($O_{z=0}$), origin moved along the z-axis ($O_{z=d}$), where d is the distance, the origin in the middle between the two Fe atoms (Fe-Fe) and the origin placed on one of the Fe atom (Fe) in the ANO-RCC-VTZP basis set.

4.3.2. [(hedta)FeOFe(hedta)]

The experimental K pre-edge of the hedta dimer has a shoulder at low energy and a more intense peak at higher energy, see Figure 14. The energy splitting between the two features is around 1.7 eV. The RASSCF spectrum also shows two distinct pre-edge features, with a more intense peak at higher energy. The energy splitting is overestimated by 0.4 eV and the low-energy peak appears more intense in the simulated spectrum. The deviation is not unreasonable considering the lack of dynamical correlation. At the double-ζ level the PT2 calculation is feasible, but there are problems to eliminate the intruder states for all possible final states, which leads to erroneous predicitions of intensity below the pre-edge. A calculation at the PT2/triple-ζ is to costly for a system of this size, especially considering the large number of final states.

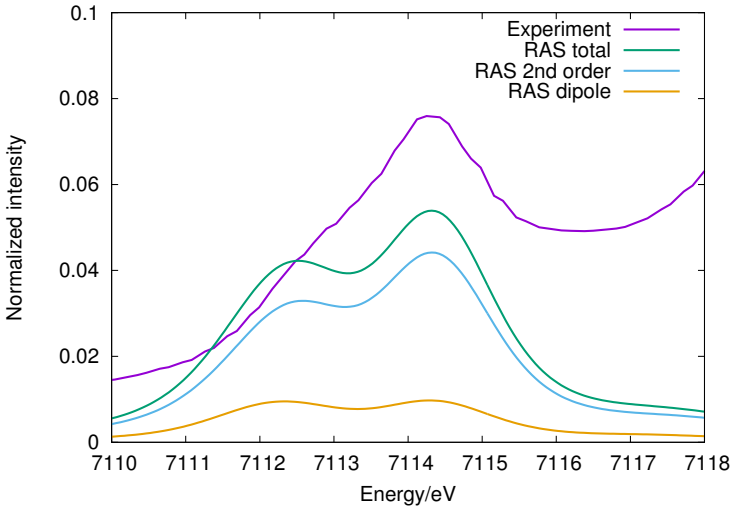

Figure 14. Experimental and RASSCF/ANO-RCC-VTZP simulated K pre-edge spectra of [(hedta)FeOFe(hedta)].

An analysis of the RASSCF spectrum shows that the contributions are almost completely dominated by the second-order (electric quadrupole) contributions. The

contribution from electric dipoles is small and equally spread between the two pre-edge features. This is slightly different from previous suggestions that the higher of the two features should have significant intensity due to increased mixing of metal 4p orbitals into the orbitals of antibonding character.[1] There is no experimental data regarding the dipole contributions, which makes it difficuly to make a proper evaluation of the simulation results, but a lack of significant dipole intensity could possibly be related to the choice of active space in the current simulation. Although there are 13 orbitals in the active space, there are no high-energy unoccupied orbitals, unlike the case for $[FeCl_4]^{1-}$ where the dipole-quadrupole ratio could be well described. [21]

5. Summary and prospects

We have presented the implementation of the origin independent quadrupole intensities in the length representation and shown the possibilities and limitations of this approach for calculating XAS intensities for complexes containing both single and multiple transition metal. While the quadrupole intensities in the length representation would be origin independent in the limit of a complete basis, we have found that this does not apply for standard basis sets available in quantum chemistry.

The problem with the length representation stems from the formulation of the origin independent intensities [22], which relies on exact cancellation order by order of the oscillator strength of the different origin dependent contributions. Since the transformation from the velocity to the length representation is not exact for quantum chemical calculations the exact cancellation of the different contributions are lost in the length representation.

For complexes with a single transition metal the length representation shows no problems compared to the velocity representation provided that the origin is placed on the transition metal. The method can also be applied to systems with multiple transistion metals provided resonable basis sets are used. However, the applicability of the method is limited by the distance between the transition metals, the size of the dipole intensities and the ratio between the dipole intensities in the length and velocity representation. A recommendation is to place the origin between the transition metals and calculate the dipole intensities in both the length and velocity representation to assess the size of the introduced error. For very large dipole intensities and distances between the transition metals beyond $6\mathring{A}$, the ratio between the dipole intensities in the length and velocity representation should not deviate by more than 10^{-3}, which may be difficult to reach. For medium to weak dipole intensities the method implemented here is capable of calculating metal dimer as Fe-O-Fe and [(hedta)FeOFe(hedta)]. While the origin cannot be randomly placed, the usual places for the origin from symmetry considerations are certainly possible.

Since the exact cancellation of order by order in the oscillator strength gives origin independence shows that the rate of convergence of the multipole expansion does not depend on where the origin is placed contrary to previous claims [26, 27]. The position of the origin only help to determine the size of the cancellation between the different contributions. As the different terms depend on the origin, the interpretation of spectra should only be done for origin-independent parts since the origin-dependent parts vary strongly even if the total is origin independent, as shown for both $[FeCl_4]^{1-}$ and Fe-O-Fe in Fig. 9 and Fig. 13.

The negative intensities first observed in [27] in the velocity representation is also here observed in the length representation. These have only been observed in

systems with large dipole oscillator strengths and only in basis sets where the ratio between the dipole oscillator strength in the length and velocity representations is large. Other basis sets therefore does not show the same unphysical behaviour. We ascribe these unphysical solutions to basis set insufficiencies which arise due to different basis sets requirement for different terms in the multipole expansion causing some term to be either over- or underestimated. For this reason it is not clear if a finite truncation of the multipole expansion always will give total positive intensities in finite basis sets.

The problems associated with origin dependence can be overcome by switching from the length to the velocity representation or even more elegantly to the exact expression as presented by List et al.[23]. The List et al.[23] approach also avoids the unphysical total negative intensities observed in [27] in the velocity representation and in the length representation in this work irrespectively of the choice of basis set.

Acknowledgement(s)

We thank Per-Åke Malmqvist for valuable suggestions on the RAS calculations. Financial support was received from the Knut and Alice Wallenberg Foundation for the project Strong Field Physics and New States of Matter (Grant No. KAW-2013.0020) and the Swedish Research Council (Grant No. 2012-3910). Computer resources were provided by SNIC trough the National Supercomputer Centre at Linköping University (Triolith) under projects snic2014-5-36, snic2015-4-71, snic2015-1-465 and snic2015-1-427.

References

[1] T.E. Westre, P. Kennepohl, J.G. DeWitt, B. Hedman, K.O. Hodgson and E.I. Solomon, J. Am. Chem. Soc. **119** (27), 6297 (1997).
[2] S. DeBeer George, P. Brant and E.I. Solomon, J. Am. Chem. Soc. **127** (2), 667 (2005).
[3] A. Roe, D. Schneider, R. Mayer, J. Pyrz, J. Widom and L. Que Jr, J. Am. Chem. Soc. **106** (6), 1676 (1984).
[4] M.H. Lim, J.U. Rohde, A. Stubna, M.R. Bukowski, M. Costas, R.Y. Ho, E. Münck, W. Nam and L. Que, Proc. Nat. Acad. Sci. USA. **100** (7), 3665 (2003).
[5] J.U. Rohde, T.A. Betley, T.A. Jackson, C.T. Saouma, J.C. Peters and L. Que, Inorg. Chem. **46** (14), 5720 (2007).
[6] M. Lundberg and T. Borowski, Coordination chemistry reviews **257** (1), 277 (2013).
[7] F.A. Lima, T.J. Penfold, R.M. van der Veen, M. Reinhard, R. Abela, I. Tavernelli, U. Rothlisberger, M. Benfatto, C.J. Milne and M. Chergui, Phys. Chem. Chem. Phys. **16** (4), 1617 (2014).
[8] B.O. Roos, P.R. Taylor and P.E.M. Siegbahn, Chem. Phys. **48** (2), 157 (1980).
[9] H. J. Aa. Jensen, P. Jørgensen and H. Ågren, The Journal of chemical physics **87** (1), 451 (1987).
[10] H. Ågren and H. J. Aa. Jensen, Chemical physics letters **137** (5), 431 (1987).
[11] H. Ågren, A. Flores-Riveros and H. J. Aa. Jensen, Physica Scripta **40** (6), 745 (1989).
[12] H. Ågren and H. J. Aa. Jensen, Chemical physics **172** (1), 45 (1993).
[13] P.Å. Malmqvist, International Journal of Quantum Chemistry pp. 479–494 (1986).
[14] J. Olsen, B.O. Roos, P. Jørgensen and H. J. Aa. Jensen, J. Chem. Phys. **89** (4), 2185 (1988).
[15] P.Å. Malmqvist, K. Pierloot, A.R.M. Shahi, C.J. Cramer and L. Gagliardi, J. Chem. Phys. **128** (20), 204109 (2008).
[16] R. Klooster, R. Broer and M. Filatov, Chemical Physics **395**, 122 (2012).
[17] I. Josefsson, K. Kunnus, S. Schreck, A. Fhlisch, F. de Groot, P. Wernet and M. Odelius, J. Phys. Chem. Lett. **3** (23), 3565 (2012).
[18] S.I. Bokarev, M. Dantz, E. Suljoti, O. Kühn and E.F. Aziz, Phys. Rev. Lett. **111** (8), 083002 (2013).

[19] R.V. Pinjari, M.G. Delcey, M. Guo, M. Odelius and M. Lundberg, J. Chem. Phys. **141** (12), 124116 (2014).
[20] R.V. Pinjari, M.G. Delcey, M. Guo, M. Odelius and M. Lundberg, J. Chem. Phys. **142** (6), 069901 (2015).
[21] M. Guo, L.K. Sørensen, R.V. Pinjari, M.G. Delcey and M. Lundberg., Phys. Chem. Chem. Phys. **18**, 3250 (2015).
[22] S. Bernadotte, A.J. Atkins and C.R. Jacob, J. Chem. Phys. **137** (20), 204106 (2012).
[23] N.H. List, J. Kauczor, T. Saue, H. J. Aa. Jensen and P. Norman, The Journal of chemical physics **142** (24), 244111 (2015).
[24] N.H. List, T. Saue and P. Norman, Molecular Physics (2016).
[25] L.K. Sørensen, R. Lindh and M. Lundberg, arXiv:1608.02399 (2016).
[26] S. DeBeer George, T. Petrenko and F. Neese, Inorg. Chim. Acta. **361** (4), 965 (2008).
[27] P. J. Lestrange, F. Egidi and X. Li, J. Chem. Phys **143**, 234103 (2015).
[28] A. Halkier, W. Klopper, T. Helgaker and P. Jørgensen, J. Chem. Phys. **111** (10), 4424 (1999).
[29] O. Christiansen, C. Hättig and J. Gauss, J. Chem. Phys. **109** (12), 4745 (1998).
[30] K.L. Bak, J. Gauss, T. Helgaker, P. Jørgensen and J. Olsen, Chem. Phys. Lett. **319** (5-6), 563 (2000).
[31] F. Aquilante, J. Autschbach, R. K. Carlson, L. F. Chibotaru, M. G. Delcey, L. De Vico, I. Fdez. Galvan, N. Ferré, L. M. Frutos, L. Gagliardi, M. Garavelli, A. Giussani, C. E. Hoyer, G. Li Manni, H. Lischka, D. Ma, P Å Malmqvist, T. Müller, A. Nenov, M. Olivucci, T. B. Pedersen, D. Peng, F. Plasser, B. Pritchard, M. Reiher, I. Rivalta, I. Schapiro, J. SegarraMarti, M. Stenrup, D. G Truhlar, L. Ungur, A. Valentini, S. Vancoillie, V. Veryazov, V. P. Vysotskiy, O. Weingart, F. Zapata, R. Lindh, Journal of Computational Chemistry **37**, 506 (2016).
[32] P.Å. Malmqvist and B.O. Roos, Chem. Phys. Lett. **155** (2), 189 (1989).
[33] P.Å. Malmqvist, B.O. Roos and B. Schimmelpfennig, Chem. Phys. Lett. **357** (3), 230 (2002).
[34] M. Douglas and N.M. Kroll, Annals of Physics **82** (1), 89 (1974).
[35] B.A. Hess, Physical Review A **33** (6), 3742 (1986).
[36] B.O. Roos, R. Lindh, P.Å. Malmqvist, V. Veryazov and P.O. Widmark, J. Phys. Chem. A. **108** (15), 2851 (2004).
[37] B.O. Roos, R. Lindh, P.Å. Malmqvist, V. Veryazov and P.O. Widmark, J. Phys. Chem. A. **109** (29), 6575 (2005).
[38] F. Aquilante, P.Å. Malmqvist, T.B. Pedersen, A. Ghosh and B.O. Roos, J. Chem. Theory. Comput. **4** (5), 694 (2008).
[39] Z. Warnke, E. Styczeń, D. Wyrzykowski, A. Sikorski, J. Kłak and J. Mroziński, Structural Chemistry **21** (2), 285 (2010).
[40] T. Yamamoto, X-Ray. Spectrom. **37** (6), 572 (2008).
[41] M.O. Krause and J. Oliver, J. Phys. Chem. Ref. Data. **8** (2), 329 (1979).